

Transmission-Reflection-Integrated Full-Space Metasurface for OAM Beam Generation

Honggang Hao, Siyao Li, Wen Huang, Yi Shen, Zonggui Li, and Ting Zhang

School of Optoelectronic Engineering, Chongqing University of Posts and Telecommunications, Chongqing, China

ABSTRACT: In this paper, a spatial-multiplexing-based transmission-reflection-integrated full-space metasurface (FS-MS) is proposed, which is applied to the generation of orbital angular momentum (OAM) beam. Using the principles of anisotropy and spatial multiplexing, the metasurface element is designed. The element consists of three dielectric substrates and four metal layers, which are of conventional cross-shaped and slotted cross-shaped construction. The designed element has the ability to independently modulate transmitted and reflected electromagnetic (EM) waves at 15 GHz. When EM waves with different polarizations are incident, the metasurface is capable of transmission at the incident x -polarized waves and reflection at the incident y -polarized waves. Using the designed element, the FS-MS was designed by combining the theories of OAM beam generation and phase superposition. The results show that the metasurface can generate the OAM beam with the topological charge of +2 in the transmission mode and +3 in the reflection mode at 15 GHz. The purity of the generated OAM beam is 78.88% in transmission mode and 72.87% in reflection mode. The metasurface proposed in this paper is characterized by the integration of transmission and reflection, which is valuable for applications in wireless communications, sensing, and imaging.

1. INTRODUCTION

In 1992, Allen et al. first experimentally demonstrated that Laguerre Gaussian beams can carry orbital angular momentum (OAM) [1]. Then, OAM-based techniques have been continuously researched and developed. Li et al. proposed metasurfaces for dual OAM beam generation, and OAM can be used as a new degree of freedom that can increase the channel capacity and solve the problem of crosstalk, which has potential applications in the field of wireless communications [2]. In the field of radar, Liu et al. proposed EM vortex imaging based on OAM, which realized good radar imaging performance [3]. For sensing applications, OAM has the potential to improve the performance of conventional object detection as well as imaging systems. For example, for rotational Doppler detection, the beam with a specific OAM index is used to illuminate the spinning object [4]. Commonly used devices for generating OAM beams are traveling wave antennas, array antennas, and metasurfaces, among which, metasurfaces have the advantage of being easy to process.

Metasurfaces are two-dimensional artificial materials composed of a subwavelength structure widely used to manipulate electromagnetic (EM) waves' amplitude, phase, frequency, or polarization. Metasurfaces have been widely used in various fields such as focusing [5], radar cross-section reduction [6], imaging [7], and communication [8–10]. The ability of the metasurface to flexibly modulate EM waves makes it a promising application. Metasurfaces can be used for OAM beam generation. In recent years, several studies have dealt with the generation of OAM beams using transmissive or reflective meta-

surfaces. Yang et al. proposed an OAM wireless communication system based on a transmissive metasurface [11]. Liao et al. proposed an OAM-generated folded transmissive array antenna [12]. Zhang et al. proposed a vortex beam generation based on a reflective metasurface [13]. Ali et al. proposed a multiband reflective array for generating OAM beams [14]. With the rapid development of modern systems, miniaturized and integrated systems have become an important development trend. To solve the problem of EM wave space utilization, full-space metasurface (FS-MS) was created. The metasurfaces designed by Huang et al. and Liu et al. can independently regulate the transmitted and reflected beams by changing the operating frequency, realizing the full-space regulation of EM waves [15, 16]. The metasurfaces designed by Li et al. control the transmission and reflection of EM waves by varying the electrical lengths of different parts of the transmission line [17]. These works demonstrate the ability of full-space metasurfaces to modulate EM waves in both directions. The fusion design of transmission and reflection breaks through the bottleneck of the design of traditional arrays in the half-space and unidirectional direction. This breakthrough effectively expands the coverage range of the communication system, enabling the establishment of reliable communication links between mobile terminals and multiple mobile terminals. Moreover, it provides a new way of thinking about the design of full-space metasurfaces for the generation of OAM beams. The large coverage of full-space metasurfaces can increase the channel capacity for wireless communication and provide more multiplexed communication links, and the study of metasurfaces with efficient full-space modulation capability is still a hot topic.

* Corresponding author: Siyao Li (s230431048@stu.cqupt.edu.cn).

Traditional transmission or reflection metasurfaces can only regulate EM waves in their respective half-space, which limits their coverage. To improve the coverage of EM waves, it is of great significance to study the transmission-reflection integrated metasurface with full-space EM coverage, which can realize the fusion design of the two radiation characteristics of transmission and reflection, break through the bottleneck of the traditional metasurface in terms of half-space and single-pointing design, and effectively expand the coverage of EM waves. To realize full-space EM regulation, the fusion design of transmission and reflection functions is realized by independently designing transmission and reflection elements.

In this paper, a transmission-reflection-integrated FS-MS design method aimed at generating OAM beams with various modes is proposed. The FS-MS element comprises three dielectric layers and four metal layers. The metasurface can generate an OAM beam with topological charge l being +2 in the transmitted half-space and an OAM beam with a topological charge l being +3 in the reflected half-space. The proposed FS-MS for OAM beam generation has the advantage of bidirectional radiation generation and has certain engineering significance in wireless communication, sensing, imaging, and other fields.

2. DESIGN OF METASURFACE ELEMENT

To achieve the FS-MS to generate OAM beams with different topological charges in transmission and reflection modes, the element should have the property of being able to independently modulate the phase in the transmission and reflection directions.

Figure 1 shows the conceptual diagram of the FS-MS. As shown in Fig. 2, the element consists of four metal layers (orange parts) separated by three dielectric substrate layers (blue parts) with a thickness h of 1 mm. The substrates are F4B with a relative permittivity of 2.65 and a loss tangent $\tan \delta$ of 0.001, and the thickness of each metal layer is 0.035 mm. The geometric parameters are $p = 8$ mm, $la = 2$ mm, $lb = 3$ mm, $lc = 1.2$ mm, $ld = 5$ mm. lx and ly are variables to control the phases of transmission and reflection, respectively.

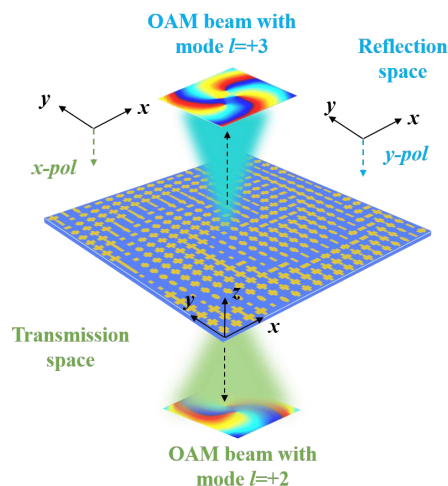


FIGURE 1. The conceptual diagram of the proposed FS-MS.

The element was analyzed using the full-wave simulation software CST Microwave Studio. Figs. 3(a) and (b) show the current distributions of the element irradiated by x -polarized and y -polarized incident waves at 15 GHz, respectively. The current distributions indicate that the x -polarized wave can pass through the element, and the y -polarized wave is reflected.

When x -polarized waves (E_i^x) are incident, different transmission phases can be obtained by adjusting lx ; when y -polarized waves (E_i^y) are incident, different reflection phases can be obtained by adjusting ly . Keeping the parameter ly constant and varying the parameter lx from 1.20 mm to 6.09 mm, the transmission phase and amplitude are shown in Fig. 4(a). Similarly, keeping the parameter lx constant and varying the parameter ly from 3.00 mm to 8.00 mm, the reflection phase and amplitude are shown in Fig. 4(b).

In the structural element, lx is aligned with the x -polarization direction of the incident wave, and ly is aligned with the y -polarization direction of the incident wave. The performance of the element is mainly modulated by lx and ly . By adjusting the parameter lx , the phase in the x -polarization direction can be regulated; by adjusting the parameter ly , the phase in the y -polarization direction can be regulated. When adjusting one of the parameters, the effect on the phase of the other orthogonal polarization direction should be minimized. To simplify the design of the metasurface, the phase needs to be discretized according to the concept of encoding the metasurface [18]. Therefore, based on the phase response, the dimensions of the parameters lx and ly can be determined. Some simulation results for elements with different lx and ly are shown in Fig. 5. Figs. 5(a)–(f) show the simulated transmission phase and amplitude for different lx (ly is fixed as 6.43 mm) and reflection phase and amplitude for different ly (lx is fixed as 6.09 mm). Figs. 5(e) and (f) show that the frequency response of the transmission element to lx is independent of the frequency response of the reflection element to ly . T_{yx} represents the y -polarized transmitted wave due to the incident x -polarized wave. R_{xy} represents the x -polarized reflected wave due to the incident y -polarized wave. Therefore, there is good isolation between the transmission element and reflection element, and the polarization purity and high efficiency of the proposed element are guaranteed. From the above results, it can be observed that by controlling the lengths of lx and ly , respectively, the phase coverage of transmission and reflection is close to 315° , and the amplitude remains above -3 dB in most cases, which is sufficient for the design of FS-MS. The above results demonstrate the independent modulation capability of the proposed element at 15 GHz, which independently realizes the phase modulation of both x -polarized and y -polarized waveforms.

Based on the above results and analyses, it can be demonstrated that the proposed FS-MS element has good transmittance and reflectance at 15 GHz, and at the same time, it can independently control the transmission phase and reflection phase of the x -polarized waves (E_i^x) and y -polarized waves (E_i^y), which meets the requirements for constructing FS-MS arrays.

Discretizing the phase gradient over the entire period with a 45° transmission phase difference as the gradient yields the eight states “T1-T8”. Similarly, the reflected phases were

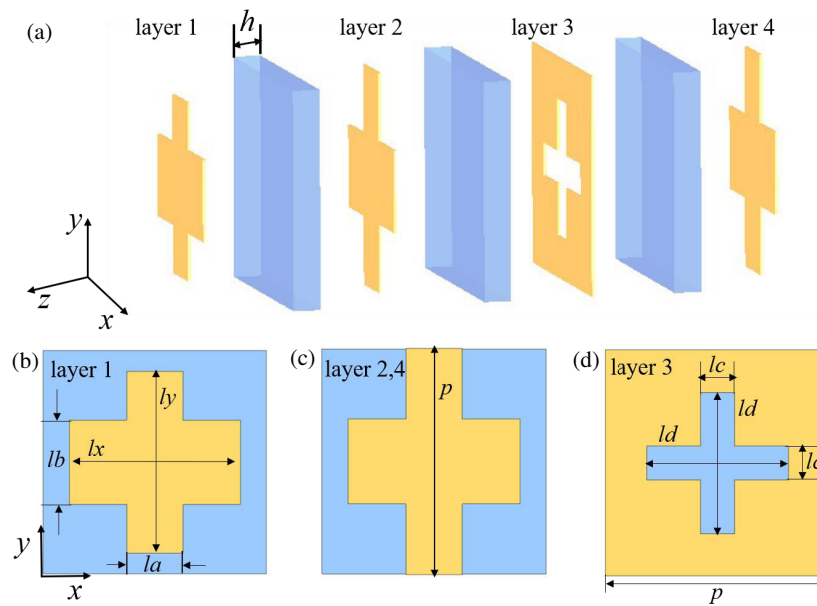


FIGURE 2. Element structure. (a) 3-D structure diagram, (b) top view of the first layer, (c) top view of the second and fourth layers, and (d) top view of the third layer.

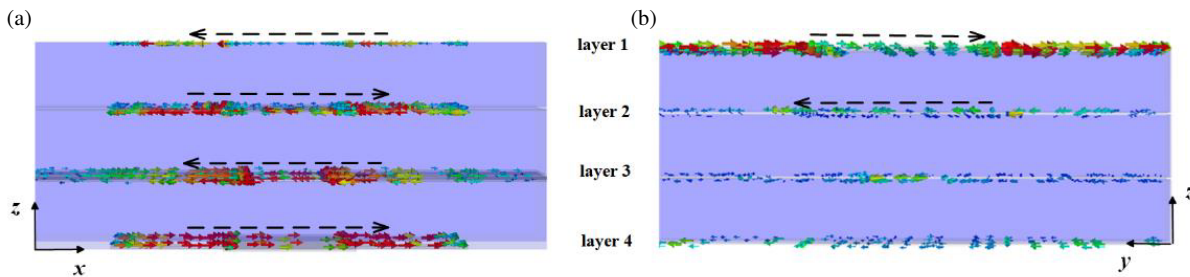


FIGURE 3. Element current distribution. (a) Under x -polarized wave incidence. (b) Under y -polarized wave incidence.

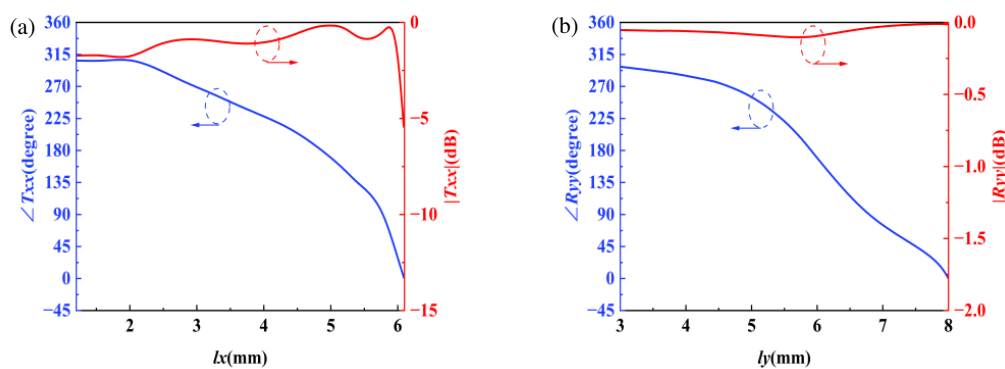


FIGURE 4. Transmission and reflection amplitude and phase. (a) The transmission amplitude and phase of the element as parameter l_x varies under x -polarized wave incidence. (b) The reflection amplitude and phase of the element as parameter l_y varies under y -polarized wave incidence.

spaced at 45° intervals, yielding eight discrete states of “R1-R8”. Fig. 6 presents the characteristic curves corresponding to the selected discrete states. It can be observed from this figure that the transmission and reflection amplitudes exceed -3 dB in most cases at 14–16 GHz, while maintaining a good linear phase response.

3. DESIGN OF FS-MS FOR GENERATING OAM BEAM

Characterized by infinite modes as well as good orthogonality between modes, OAM has great advantages in significantly expanding the channel capacity and spectral efficiency without increasing the spectral resources [19], which provides a new degree of freedom for modulation and information bearing of EM

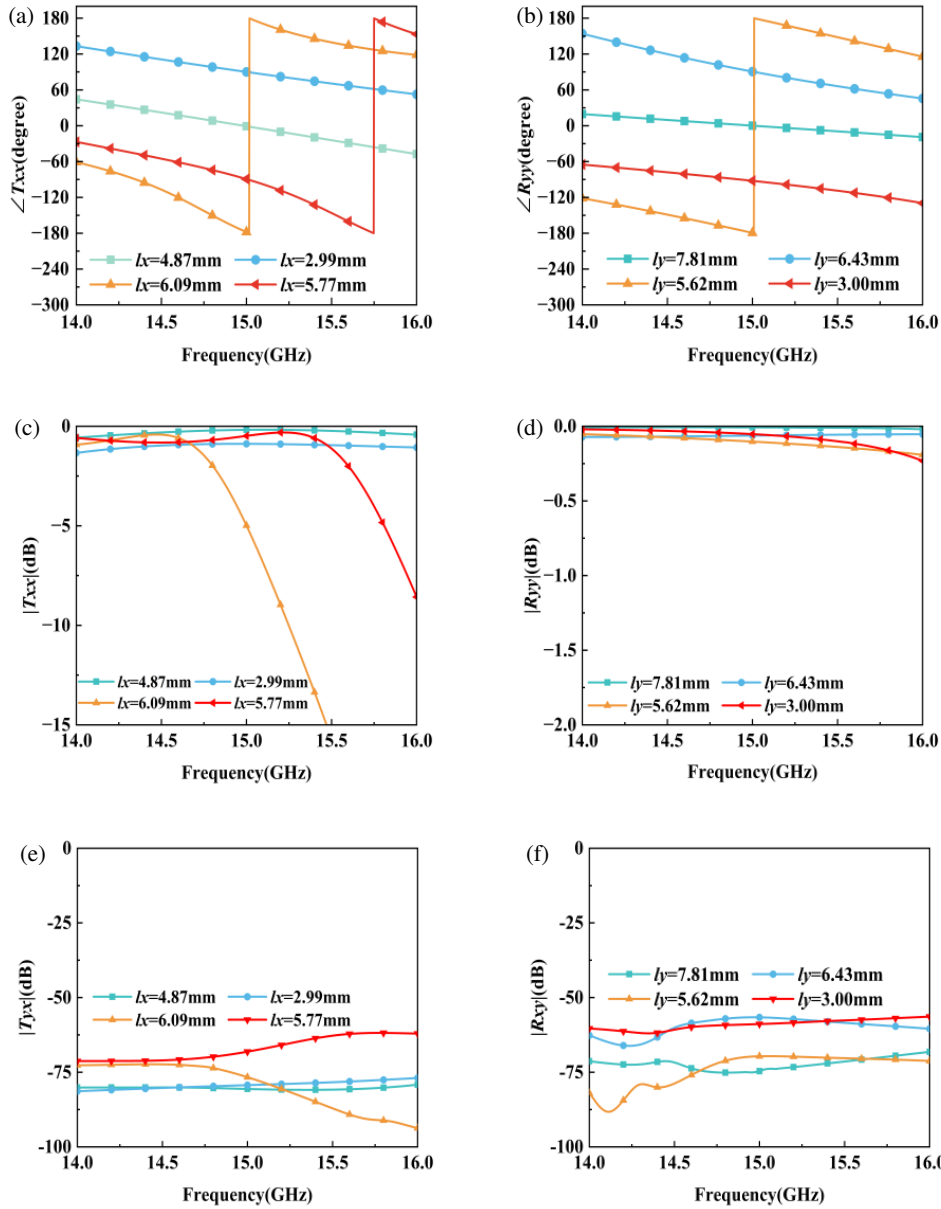


FIGURE 5. Transmission and reflection phase and amplitude with different l_x and l_y . (a) Phase of T_{xx} . (b) Phase of R_{yy} . (c) Amplitude of T_{xx} . (d) Amplitude of R_{yy} . (e) Amplitude of T_{yx} . (f) Amplitude of R_{xy} .

waves. Based on the phase superposition principle, the metasurface can be made to generate OAM beams. OAM beams show promising applications in many fields. For FS-MS, the transmission and reflection phases need to be independently modulated to generate vortex beams carrying OAM modes.

To demonstrate the EM wave modulation capability of the element, an FS-MS consisting of 20×20 elements with total sizes of $160 \text{ mm} \times 160 \text{ mm} \times 3.14 \text{ mm}$ is designed. To simultaneously and independently modulate the transmitted and reflected EM waves, it is necessary to arrange the phase distribution of the metasurface accordingly for the transmitted and reflected parts, respectively. Since the feed horn emits a spherical wave, the spherical wave needs to be compensated and corrected to a plane wave. ϕ_f is the phase compensation for the

distance between the metasurfaces and the feed horn, position $(f_x, f_y, f_z) = (0, 0, 128) \text{ mm}$.

$$\phi_f = (2\pi/\lambda) \sqrt{x_{mn}^2 + y_{mn}^2 + f_z^2} \quad (1)$$

The required phase compensation ϕ_L for the transmissive and reflection elements at position $(x_{mn}, y_{mn}, 0)$ can be calculated by Equations (2) and (3), where ϕ_{vox} is used to generate the vortex beam, and l is the topological charge of the vortex beam. The phase superposition process and the final phase distribution of the OAM beam with $l = +2$ are illustrated in Figs. 7(a)–(c), and it can be observed that the required phase of the OAM beam generator with mode number $l = +2$ gradually increases along the counterclockwise direction, undergoing two changes from 0° to 360° . Similarly, the phase superposi-

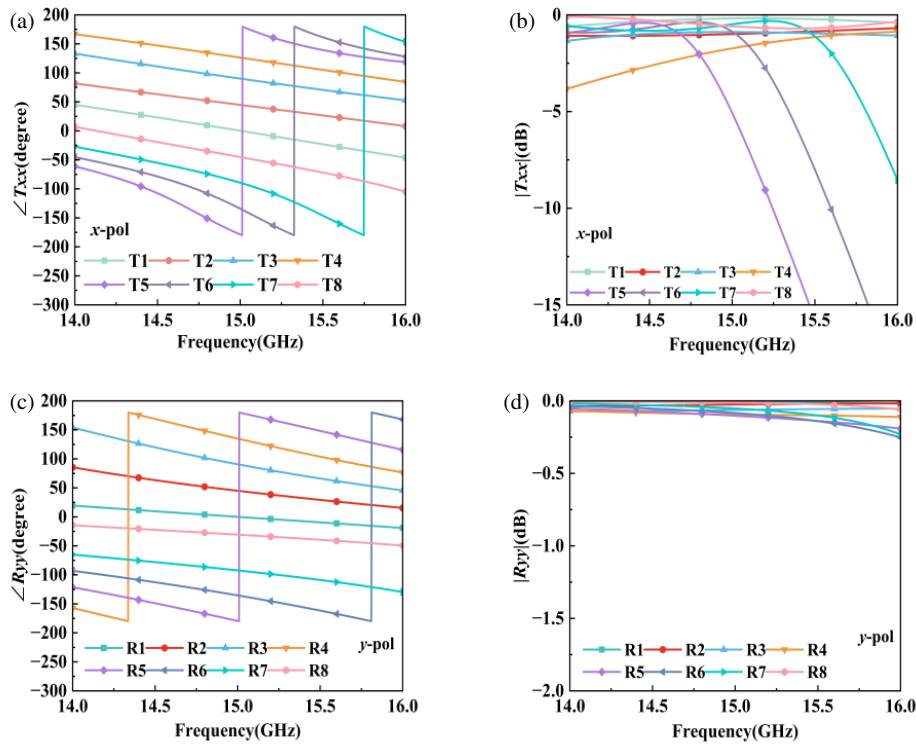


FIGURE 6. Transmission and reflection performances of elements. (a) Transmission phase under x -polarized wave incidence. (b) Transmission amplitude under x -polarized wave incidence. (c) Reflection phase under y -polarized wave incidence. (d) Transmission amplitude under y -polarized wave incidence.

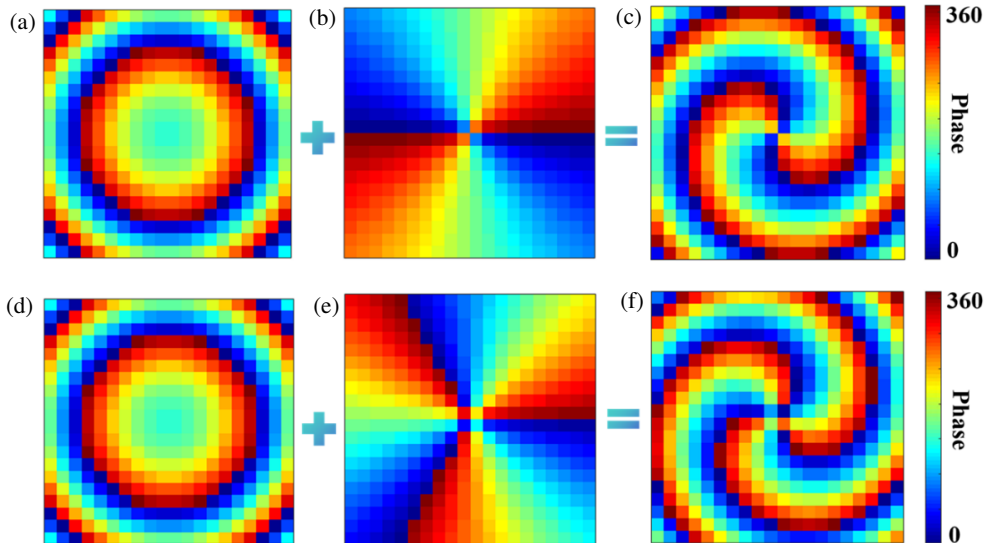


FIGURE 7. Phase distribution on the metasurface. (a) Feed horn phase at 15 GHz. (b) OAM phase at 15 GHz with mode $l = +2$. (c) Final phase at 15 GHz with mode $l = +2$. (d) Feed horn phase at 15 GHz. (e) OAM phase at 15 GHz with mode $l = +3$. (f) Final phase at 15 GHz with mode $l = +3$.

tion process and the final phase distribution of the OAM beam with $l = +3$ are illustrated in Figs. 7(d)–(f).

$$\phi_L(x_{mn}, y_{mn}) = \phi_f + \phi_{vox} \quad (2)$$

$$\phi_{vox} = l \cdot \arctan\left(\frac{y_{mn}}{x_{mn}}\right) \quad (3)$$

Through Equations (1), (2), and (3), computations are conducted to determine the necessary phases for the reflective and transmissive elements of each element. Subsequently, a metasurface array is composed based on the discretized elements.

As shown in Fig. 8, the OAM beam is generated at the 15 GHz frequency point. When x -polarized waves (E_i^x) and

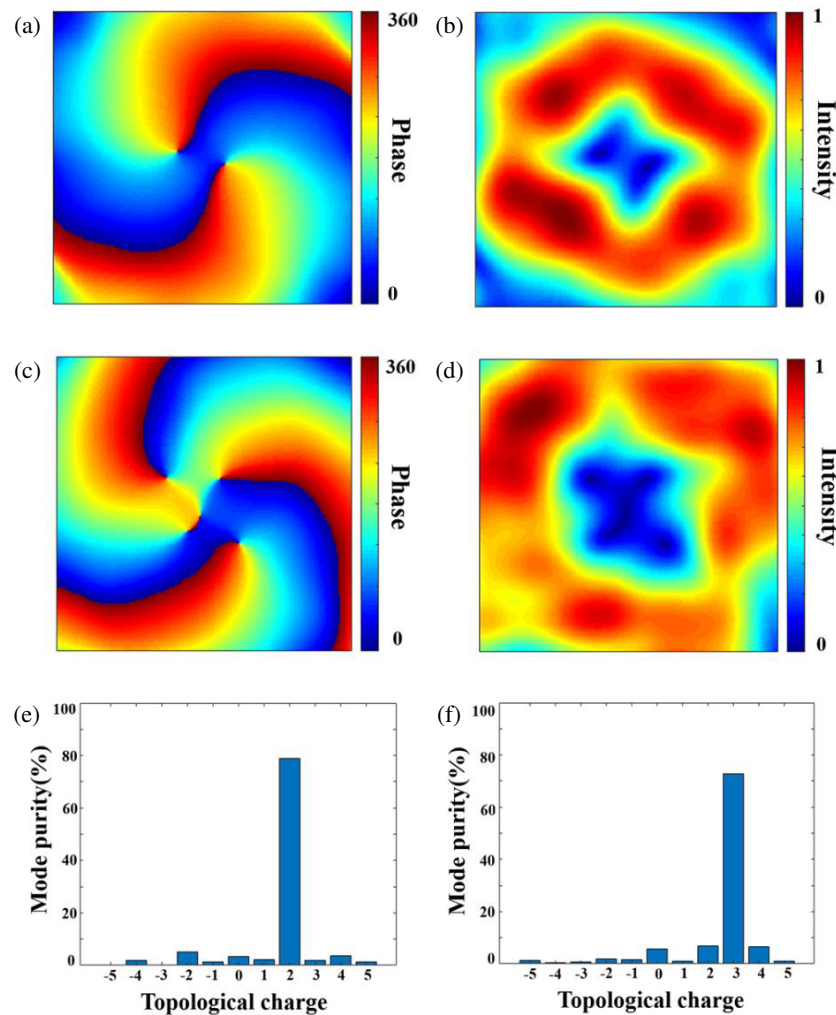


FIGURE 8. The intensity of OAM beam. (a) Phase distribution of electric field with mode $l = +2$. (b) Electric field intensity distribution with mode $l = +2$. (c) Phase distribution of electric field with mode $l = +3$. (d) Electric field intensity distribution with mode $l = +3$. (e) Mode purity with mode $l = +2$. (f) Mode purity with mode $l = +3$.

y -polarized waves (E_i^y) are incident, the electric field phase and intensity are recorded in the xoy plane at a distance of $z = 300$ mm from the metasurface in the transmission and reflection half-space, respectively. As can be seen from Figs. 8(a) and (c), the spiral phase distribution can be clearly observed in the xoy plane, and the number of spiral phase arms is 2 and 3, respectively. Figs. 8(b) and (d) show the electric field intensity, in which the doughnut-style circular electric field intensity is an intrinsic property due to the centrosymmetric phase distribution of the OAM beam generator, and it can be seen that a cavity with a very weak electric field strength is formed in the central region, which is in accordance with the EM properties of vortex waves. The OAM mode purity can be calculated from the Laguerre-Gaussian model [20], by which the mode purity map of the generated vortex beam can be obtained, as shown in Figs. 8(e) and (f). The results show that the dominant mode of the OAM beam in the transmission mode is $l = +2$ with a mode purity of 78.88%, while all other noise mode numbers are below 6%. In the reflection mode, the dominant mode of the OAM

beam is $l = +3$ with a mode purity of 72.87%, while all other noise modes are below 7%. Moreover, due to the differences in transmission and reflection amplitudes between the individual elements in the designed metasurface, the purity of the modes is not particularly high. The purity can be improved by reducing the amplitude difference between the elements and increasing their transmission and reflection amplitudes. Theoretically, as the distance increases, the OAM beam tends to diverge slightly, and its intensity diminishes. In practical communication links, the loss of the signal may increase due to factors such as atmosphere and obstacles, so it is of great significance to further reduce the loss of the metasurface.

As mentioned before, FS-MS is characterized by bidirectional radiation, which can be applied in various scenarios, such as tunnels, underground passages, indoor wireless communications, and other areas with great application potential, and improves the space utilization rate compared with the traditional EM wave half-space modulation of the metasurface. This paper takes the generation of OAM beams as an example to illustrate

TABLE 1. Comparison of the proposed metasurface with other works.

| Ref. | [25] | [26] | [27] | [16] | This work |
|---------------------------------|--------------------|-------------|------------------------------|--------------|-------------------------|
| Frequency (GHz) | 10 | 19 | 10 | 18/12 | 15 |
| Metal layers | 2 & the air spacer | 2 | 3 & the metallized via-holes | 5 | 4 |
| Functionalities | OAM | OAM | OAM | OAM/Focusing | OAM |
| Periodicity (λ_0) | 0.6 | 0.4 | 0.46 | 0.35 | 0.4 |
| Aperture size (λ_0^2) | 158.76 | 315.42 | 100 | 217.70 | 64 |
| Polarization | LP/CP | LP/CP | LP | LP/CP | LP |
| Aperture efficiency (%) | No | 3.36 | 2.95/1.74 | No | 4.93/4.35 |
| OAM mode | $l = +1$ | $l = \pm 1$ | $l = +1/l = +2$ | $l = +2$ | $l = +2/l = +3$ |
| Mode purity (%) | $\geq 64/\geq 60$ | ≥ 81.5 | ≥ 80 | No | $\geq 78.88/\geq 72.87$ |

the FS-MS generation process. Using the element designed, based on the phase superposition theory, it can be further extended to generate focusing beams, Bessel beams, and the realization of radar cross-section reduction and other functions.

A comparison of the key metrics between the proposed metasurface and other metasurfaces is given in Table 1. This design has stable performance, simple structure, and low cost which provides a good idea to enhance the full-space modulation capability of the metasurface. Compared with the traditional single transmission-type or reflection-type metasurfaces, the FS-MS proposed in this paper is characterized by the bi-directional modulation of EM waves, which broadens the coverage of EM waves.

4. CONCLUSION

An FS-MS for generating OAM beams is designed. The metasurface can independently generate OAM beams with different orbital angular momentum modes according to the polarization states of the transmitted and reflected waves. In addition, the proposed FS-MS is characterized by bidirectional radiation and polarization modulation, which is of great value for applications in wireless communication, sensing, and imaging. This work is passive and can only generate fixed OAM modes. If active control is incorporated, different orders of OAM beams can be achieved to enhance communication capacity.

ACKNOWLEDGEMENT

This work was supported by Chongqing Natural Science Foundation General Program (CSTB2022NSCQ-MSX0960); Scientific and Technological Research Program of Chongqing Municipal Education Commission (KJQN202300611).

DATA AVAILABILITY

The authors confirm that the data supporting the findings of this study are available within the article.

DISCLOSURES

The authors declare no conflicts of interest.

REFERENCES

- [1] Allen, L., M. W. Beijersbergen, R. J. C. Spreeuw, and J. P. Woerdman, "Orbital angular momentum of light and the transformation of Laguerre-Gaussian laser modes," *Physical Review A*, Vol. 45, No. 11, 8185, Jun. 1992.
- [2] Li, Z., S. Li, G. Huang, X. Liu, B. Han, and X. Cao, "Digital coding transmissive metasurface for dual-OAM-beam Generation," in *2022 International Applied Computational Electromagnetics Society Symposium (ACES-China)*, 1–2, Xuzhou, China, Dec. 2022.
- [3] Liu, H., Y. Wang, J. Wang, K. Liu, and H. Wang, "Electromagnetic vortex enhanced imaging using fractional OAM beams," *IEEE Antennas and Wireless Propagation Letters*, Vol. 20, No. 6, 948–952, Jun. 2021.
- [4] Liu, K., Y. Cheng, X. Li, and Y. Gao, "Microwave-sensing technology using orbital angular momentum: Overview of its advantages," *IEEE Vehicular Technology Magazine*, Vol. 14, No. 2, 112–118, Jun. 2019.
- [5] Wang, X., M. S. Tong, and G.-M. Yang, "Multifocus multinull near-field transmitting focused metasurface," *IEEE Transactions on Antennas and Propagation*, Vol. 71, No. 4, 3172–3182, Apr. 2023.
- [6] Li, Z. and J. Gao, "Radar cross section reduction based on disordered metasurface," in *2024 International Conference on Electromagnetics in Advanced Applications (ICEAA)*, 239–239, Lisbon, Portugal, Sep. 2024.
- [7] Gao, S., H. Ma, S. Wei, H. Liu, and G. Wang, "3D imaging method based on digital coding metasurface with unknown mutual coupling," *IEEE Transactions on Computational Imaging*, Vol. 8, 808–821, Aug. 2022.
- [8] Kumari, M., A. Sharma, and S. Chaudhary, "High-speed spiral-phase donut-modes-based hybrid FSO-MMF communication system by incorporating OCDMA scheme," Vol. 10, No. 1, 94, 2023.
- [9] Anuranjana, S. Kaur, R. Goyal, and S. Chaudhary, "1000 Gbps MDM-WDM FSO link employing DP-QPSK modulation scheme under the effect of fog," *Optik*, Vol. 257, 168809, May 2022.
- [10] Amphawan, A., S. Chaudhary, and T.-K. Neo, "Hermite-Gaussian mode division multiplexing for free-space optical interconnects," *Advanced Science Letters*, Vol. 21, No. 10, 3050–3053, Oct. 2015.
- [11] Yang, H., S. Zheng, H. Zhang, N. Li, D. Shen, T. He, Z. Yang, Z. Lyu, and X. Yu, "A THz-OAM wireless communication system based on transmissive metasurface," *IEEE Transactions on*

- Antennas and Propagation*, Vol. 71, No. 5, 4194–4203, May 2023.
- [12] Liao, D., X. Ren, L. Jing, M. Li, H. Chen, and Z. Wang, “Chiral metasurface enabled circularly polarized OAM-generating folded transmitarray antenna with high-gain low-profile and broadband characteristics,” *IEEE Transactions on Antennas and Propagation*, Vol. 71, No. 6, 4737–4746, Jun. 2023.
- [13] Zhang, T., X. Sun, Y. Zhang, and L. Liu, “Ultra-wideband millimeter-wave vortex beam generation based on reflective pancharatnam-berry phase metasurface,” *Journal of Communications and Information Networks*, Vol. 8, No. 4, 349–356, Dec. 2023.
- [14] Ali, A., M. Khalily, T. Brown, and R. Tafazolli, “Multi-band dual-beams reflectarray for mode and polarization multiplexing of OAM beams,” in *2023 IEEE International Symposium on Antennas and Propagation and USNC-URSI Radio Science Meeting (USNC-URSI)*, 1335–1336, Portland, OR, USA, Jul. 2023.
- [15] Huang, Y., C. He, and W. Zhu, “Ultrathin multifunctional transmission-reflection integrated metasurface,” in *2023 IEEE MTT-S International Microwave Workshop Series on Advanced Materials and Processes for RF and THz Applications (IMWS-AMP)*, 1–3, Chengdu, China, Nov. 2023.
- [16] Liu, X., Z. Yan, E. Wang, X. Zhao, T. Zhang, and F. Fan, “Bifunctional full-space metasurface combining Pancharatnam-Berry and propagation phases,” *IEEE Antennas and Wireless Propagation Letters*, Vol. 21, No. 10, 2110–2114, Oct. 2022.
- [17] Li, G., H. Shi, J. Yi, B. Li, A. Zhang, and Z. Xu, “Transmission-reflection-integrated metasurfaces design for simultaneous manipulation of phase and amplitude,” *IEEE Transactions on Antennas and Propagation*, Vol. 70, No. 7, 6072–6077, Jul. 2022.
- [18] Cui, T. J., M. Q. Qi, X. Wan, J. Zhao, and Q. Cheng, “Coding metamaterials, digital metamaterials and programmable metamaterials,” *Light: Science & Applications*, Vol. 3, No. 10, e218, Oct. 2014.
- [19] Yao, A. M. and M. J. Padgett, “Orbital angular momentum: Origins, behavior and applications,” *Advances in Optics and Photonics*, Vol. 3, No. 2, 161–204, Jun. 2011.
- [20] Siegman, A. E., *Lasers*, University Science Books, 1986.
- [21] Ishfaq, M., X. Li, Z. Qi, W. Zhao, A. Aziz, L. Qiu, and S. Memon, “A transmissive metasurface generating wideband OAM vortex beam in the Ka-band,” *IEEE Antennas and Wireless Propagation Letters*, Vol. 22, No. 8, 2007–2011, May 2023.
- [22] Yu, Z., T. Zhao, S. Yue, H. Li, and H. Zhang, “Quantification phase gradient near-field focusing metasurface for microwave wireless power transfer system,” *IEEE Antennas and Wireless Propagation Letters*, Vol. 23, No. 6, 1944–1948, Mar. 2024.
- [23] Du, G., D. Wang, X. Sun, and Y. Zhao, “Design of a reflective metasurface for near-field focusing,” in *2021 IEEE International Symposium on Antennas and Propagation and USNC-URSI Radio Science Meeting (APS/URSI)*, 323–324, Singapore, Feb. 2022.
- [24] Guo, X., X. Li, Y. Huang, K. Luo, H. Zhu, Z. Akram, and Z. Qi, “Design of wideband vortex reflectarray based on pancharatnam-berry metasurface,” in *2021 IEEE MTT-S International Wireless Symposium (IWS)*, 1–3, Nanjing, China, Aug. 2021.
- [25] Meng, X.-S., J.-J. Wu, Z.-S. Wu, T. Qu, and L. Yang, “Design of multiple-polarization reflectarray for orbital angular momentum wave in radio frequency,” *IEEE Antennas and Wireless Propagation Letters*, Vol. 17, No. 12, 2269–2273, Sep. 2018.
- [26] Bian, C., D. Zhou, H. Yang, H. Deng, D. Lv, D. Zhang, and Y. Zhang, “Multiple-polarization multibeam vortex wave generator with high-gain and low-profile characteristics,” *IEEE Transactions on Antennas and Propagation*, Vol. 72, No. 1, 1009–1014, Sep. 2023.
- [27] Liu, B., S.-W. Wong, K.-W. Tam, X. Zhang, and Y. Li, “Multifunctional orbital angular momentum generator with high-gain low-profile broadband and programmable characteristics,” *IEEE Transactions on Antennas and Propagation*, Vol. 70, No. 2, 1068–1076, Sep. 2021.